range about the value of R where the two curves intersect (R_c). The collisional energy at which detachment should take place would be given as $E^-(R_c) - D_e(BA^-)$, where D_e is the dissociation energy of BA^-. In such transitions between a continuum nuclear motion state of the anion and a bound or continuum nuclear motion state of the neutral, the above mathematical treatment must be modified to take into consideration the scattering nature of χ_n^-. However, the qualitative arguments advanced above should still remain valid.

Clearly there is a wide variety of physical processes involving electron loss induced by some kind of nuclear motion (vibration, rotation, or collisional impact). Autoionization of molecular Rydberg states, Penning ionization of electronically excited atoms or molecules, and vibration-rotation-induced detachment of anions and merely three special cases which are likely to be of wide interest to chemists. Because of the recent observation of electron detachment in benzyl anion caused by the absorption of IR radiation, it is timely to consider the quantum mechanical basis in terms of which one can understand such behavior. It is hoped that the three propensity rules given in section II of this paper will stimulate further experimental research into this problem. It is our feeling that work on diatomic molecular anions (where Q can only be the interatomic distance) should be examined first. For polyatomic molecules, the observation of vibration-induced detachment is more difficult to interpret because of the multidimensional nature of the anion and neutral potential-energy surfaces. By testing the model given here on diatomics or small polyatomics, one can determine its range of validity. Then, if this model is successful, it can be used to suggest and interpret experiments involving polyatomic species.

At present, the experimental methods[1] employed to study vibration-induced detachment do not permit the determination of the anion vibrational level ϵ_n^- from which one is detaching. The intense infrared laser light sources used probably populate high vibrational levels of many models of the anion. The pressure used in the ICR laser detachment experiments[1] are so low and the infrared radiative lifetimes so long ($\sim 10^{-3}$ s) that vibrationally excited anions cannot lose their energy. As a result, the laser pumping eventually excites, by a stepwise mechanism, vibrational levels which are high enough in energy to detach. If the laser fluence is high enough, the population of these higher vibrational levels will be maintained and *eventually* (although perhaps with slow rate) electrons will detach. Thus, the only control one has for indirectly determining which vibrational levels are detaching is the laser fluence. Clearly this situation is not entirely satisfactory, and much remains to be done in the way of experimental development.

Acknowledgment. I gratefully acknowledge the financial support of the National Science Foundation (Grant CHE 79-06645) and the donors of the Petroleum Research Fund, administered by the American Chemical Society (Grant 12720-AC6). I also wish to acknowledge very useful interactions with Professor John I. Brauman and his research group at Stanford.

Structures and Properties of Organic Liquids: *n*-Alkyl Ethers and Their Conformational Equilibria[1]

William L. Jorgensen*[2] and Mustafa Ibrahim

Contribution from the Department of Chemistry, Purdue University, West Lafayette, Indiana 47907. *Received November 17, 1980*

Abstract: Statistical mechanics simulations have been carried out for liquid dimethyl ether (DME) and methyl ethyl ether (MEE) at their boiling points and for liquid diethyl ether (DEE) at 25 °C. The intermolecular interactions were described by Coulomb and Lennard-Jones terms in the TIPS format. The internal rotations about the central CO bonds in the MEE and DEE monomers were also included, using potential functions derived from ab initio molecular orbital calculations. Optimization led to the interesting result that the dihedral angle for the gauche conformer in MEE occurs at ca. 85° in accord with electron diffraction data. A key finding is that the conformational equilibria for MEE and DEE are essentially unaffected by transfer from the gas phase to the pure liquids at the normal densities. The thermodynamic and detailed structural results for the liquids are also thoroughly analyzed. Excellent agreement is found with experiment for the computed heats of vaporization of all three liquids. A simulation of liquid DME under constant pressure conditions yielded a density within 4% of the experimental value which provides further support for the validity of the TIPS model. The liquids are disordered with high coordination numbers and no obvious repeating polymeric units. Trends in the structures and properties as a function of monomer size are discussed.

I. Introduction

The traditional quantum mechanical studies of organic theoreticians are applicable primarily to problems of structure and reactivity in the gas phase. The need for expanding the scope to condensed phases is apparent since most experimental organic chemistry is performed in solution and because solvent effects are often profound. Consequently, a theoretical program for the systematic investigation of organic chemistry in the liquid state has been undertaken in this laboratory. Much of the initial work has focused on the generation and suitability of the necessary intermolecular potential functions which are at the heart of statistical mechanics simulations of fluids. A set of transferable intermolecular potential functions (TIPS) has been obtained for water, alkanes, alcohols, ethers, and alkyl chlorides.[3-6] The TIPS have proven particularly successful in simulations of a variety of pure organic liquids including methanol,[4] ethanol,[5] *n*-butane,[6] and 1,2-dichloroethane (DCE).[6] The computed thermodynamic and structural data were found to be in good agreement with the available experimental results including X-ray and infrared data. The nature of the computations also provides additional detailed

(1) Quantum and Statistical Mechanical Studies of Liquids. Part 17.

(2) Camille and Henry Dreyfus Foundation Teacher-Scholar, 1978-1983; Alfred P. Sloan Foundation Fellow, 1979-1981.

(3) Jorgensen, W. L. *J. Am. Chem. Soc.* **1981**, *103*, 335.

(4) Jorgensen, W. L. *J. Am. Chem. Soc.* **1981**, *103*, 341.

(5) Jorgensen, W. L. *J. Am. Chem. Soc.* **1981**, *103*, 345.

(6) Jorgensen, W. L.; Binning, R. C.; Bigot, B. *J. Am. Chem. Soc.*, in press.

0002-7863/81/1503-3976$01.25/0

Table I. TIPS Parameters for Alkyl Ethers[a]

site	q	$A^2 \times 10^{-4}$	C^2
O	−0.50	50	600
CH_3	*b*	795	2400
CH_2	*b*	729	1825
CH	*b*	680	1150
C	*b*	610	800

[a] Units are for q (electrons), A^2(kcal Å^{12}/mol) and C^2 (kcal Å^6/mol). e^2 in eq 1 is 332.17752 kcal Å/mol. [b] Charges on the alkyl groups adjacent to the ether oxygen are +0.25 e. More remote alkyl groups are taken as neutral, q = 0.

insights into the physical and energetic structures of the fluids through distribution functions for coordination numbers, hydrogen bonding, bonding energies, and other properties.

In order to expand the studies of pure solvents and to further test the TIPS approach, the results of liquid simulations for the three simplest alkyl ethers, dimethyl ether (DME), methyl ethyl ether (MEE), and diethyl ether (DEE), are reported here. Ethers are used as dipolar aprotic solvents whose great utility in organic synthesis stems from their ability to strongly solvate alkali cations leaving the counteranions relatively free for reactions. The most widely employed ether solvents are DEE, 1,2-dimethoxyethane, and tetrahydrofuran (THF), while DME and MEE are less common due to their low boiling points. Clearly, the simulations for pure liquids are also needed as a foundation for studies of solvent effects in dilute solutions and to establish the viability of the theoretical methods.

The computations for the ethers contain many novel features. Particular attention is paid to the conformational equilibria for MEE and DEE. The necessary intramolecular rotational potential functions are obtained from ab initio molecular orbital calculations. The computed results are in accord with the experimentally observed dihedral angle of 85° for the gauche conformer of MEE. A key finding is that the condensed phase effects on the conformational equilibria for the ethers at the normal densities are negligible. Detailed analyses of the structures and thermodynamic characteristics of the liquids are also provided. Trends dependent on alkyl group size are apparent. Although the structure of DME reveals the influence of intermolecular Coulombic attractions, the effect is diminished as the alkyl groups are elaborated.

Complementing the simulations at constant volume, a Monte Carlo calculation for DME at constant pressure was carried out. This established that the TIPS potentials yield a density for DME within 4% of the experimental value. Good agreement is also obtained between theory and experiment for the heats of vaporization.

To begin, the development and characteristics of the inter- and intramolecular potential functions for ethers are described. The methodology and results for the liquid simulations are then presented.

II. Potential Functions

A. Intermolecular. The intermolecular interactions are described by potential functions in the TIPS format.[3] Interaction sites are located on the oxygen and carbon atoms in the ethers with the alkyl hydrogens implicit. Thus, DME, MEE, and DEE have three, four, and five interaction sites, respectively. Standard geometries based on microwave data[7] and reported previously[3] were used in the simulations. Specifically, r(CO) = 1.410 Å, $r(CC_0)$ = 1.516 Å, ∠COC = 112.0°, and ∠CCO = 109.47°.

The sites interact intermolecularly via Coulomb and Lennard-Jones terms (eq 1). The A and C parameters for alkyl

$$\Delta E_{ab} = \sum_i^{\text{on } a} \sum_j^{\text{on } b} \frac{q_i q_j e^2}{r_{ij}} + \frac{A_i A_j}{r_{ij}^{12}} - \frac{C_i C_j}{r_{ij}^{6}} \qquad (1)$$

groups have remained unchanged from the previous studies as summarized in Table I.[3-6] Preliminary parameters for ether oxygen were also obtained in the earlier work;[3] however they were based primarily on the dimerization energy for the linear water–DME dimer. The resultant charge for ether oxygen was −0.58 e which gives a dipole moment of 2.20 D for the ethers when the standard geometries are used. In the TIPS model, the charge on oxygen is balanced by opposite charges of half the size on the adjacent alkyl groups. The magnitude of the charges seemed somewhat too large since the dipole moment for alcohols in the TIPS model is 2.21 D,[3] while in the gas phase alcohols have dipole moments about 0.5 D greater than ethers (ca. 1.80 D vs. 1.30 D). Consequently, the charge for ether oxygen has been reduced to −0.50 e in this study which yields a dipole moment of 1.89 D. The A parameter was not changed and C^2 was reduced from 625 to 600 which is now the same as for alcohols. As discussed below, this choice of parameters, summarized in Table I, yields very good thermodynamic results for the liquid ethers.

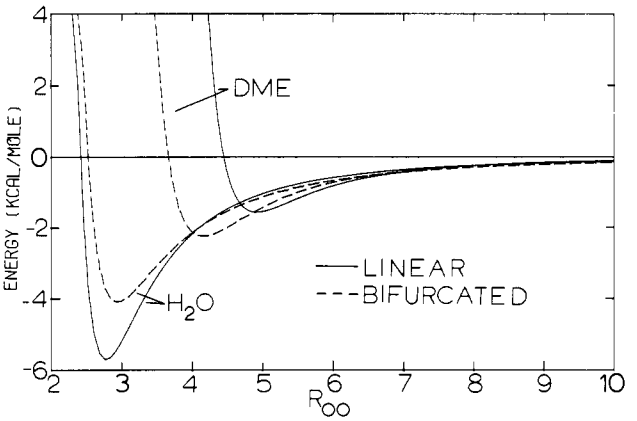

Figure 1. Variation of the dimerization energy with OO separation for the linear and bifurcated water dimers and dimethyl ether (DME) dimers. Results are from the TIPS potentials.

Table II. TIPS Results for Dimers[a]

dimer	r(OO), Å	θ, deg	$-\Delta E$, kcal/mol
linear H_2O	2.78	27	5.70
linear DME	4.91	32	1.55
cyclic H_2O	2.82	41	4.31
cyclic DME	4.28	63	1.38
bifurcated H_2O	2.94		4.09
bifurcated DME	4.16		2.24

[a] See ref 3 for definition of the geometrical variables.

Of course, the dimerization energy for the water–DME dimer has been raised from −5.70 to −4.79 kcal/mol which is in poorer accord with the ab initio 6-31G* estimate, −5.73 kcal/mol. It is not accidental that a larger charge is needed on ether oxygen when it is interacting with a hydrogen bond donor than when it is interacting with another ether. Greater polarization occurs in the hydrogen bonded complexes due to the far shorter intermolecular distances and stronger interactions. The latter points are illustrated in Figure 1 and Table II. The figure shows the dependence of the dimerization energies on OO separation in the linear and bifurcated water and DME dimers, using the TIPS. The minimum for the linear water dimer has an OO distance of 2.8 Å and a bonding energy of 5.7 kcal/mol, while the lowest energy form for the DME dimer is bifurcated with an OO distance of 4.1 Å and a bonding energy of 2.2 kcal/mol. The differences between liquid water and ethers follow largely from Figure 1; ether molecules simply cannot get close enough to have attractive enough interactions to yield a highly structured liquid.

Although the charge change discussed above is not dramatic, it indicates the desirability of incorporating polarization into the next generation of TIPS. This is particularly true for hydrogen bonding systems; however polarization is less significant for pure liquid hydrocarbons and dipolar aprotic solvents due to the larger intermolecular separations.

(7) Harmony, M. D.; Laurie, V. W.; Kuczkowski, R. L.; Schwendeman, R. H.; Ramsay, D. A.; Lovas, F. J.; Lafferty, W. J.; Maki, A. G. *J. Phys. Chem. Ref. Data Ser.* **1979**, *8*, 619.

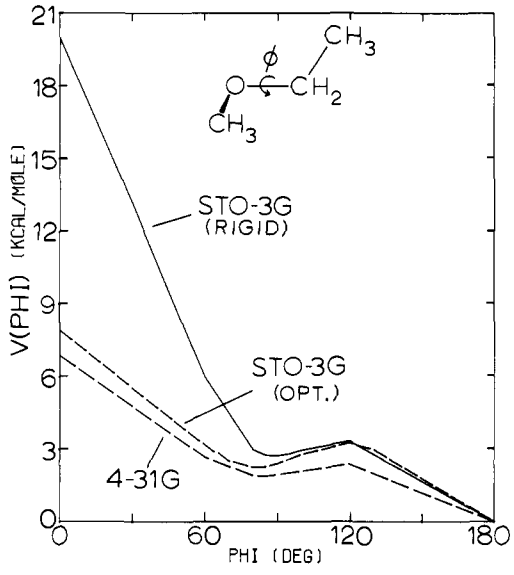

Figure 2. Potential functions for internal rotation about the central CO bond in methyl ethyl ether (MEE) from ab initio calculations.

B. Intramolecular. Besides the intermolecular interactions it is also obviously important to include the principal internal rotations about the skeletal bonds in simulations of organic liquids. This requires corresponding potential functions dependent on the dihedral angles. Such potentials were previously included in the studies of the alcohols, *n*-butane, and DCE.[4-6] MEE is similar to these cases in that there is only one principal internal rotation, i.e., about the central CO bond in the monomer. DEE presents a new challenge since the rotational potential is a function of the dihedral angles about both CO bonds.

Although internal rotation in ethers has been studied via molecular mechanics,[8a] the form of the potentials is not suitable for incorporation into the present statistical mechanics calculations and the experimental basis for the molecular mechanics functions was limited. Consequently, internal rotation in MEE and DEE has been investigated with ab initio molecular orbital methods that are known to be particularly successful for such problems.[9,10] All computations were performed with the GAUSSIAN/76 program, using the minimal STO-3G and split-valence 4-31G basis sets.[11]

Initially, STO-3G calculations were executed for MEE, using rigid rotation, the standard geometries described above, CH bond lengths of 1.09 Å, HCC angles of 109.47°, and staggered hydrogens. The computed potential, $V(\phi)$, is given by the solid curve in Figure 2. Trans and gauche minima were found at $\phi = 180°$ and 90°, respectively. The latter angle was surprising since gauche rotamers are usually near 60°. In fact, this typical value has been assumed in related theoretical studies on internal rotation in dimethoxymethane.[12] This issue is discussed further below.

As demonstrated previously, the potential is much improved if flexible rotation is permitted.[9,10] Thus, for ten points on the surface the CCO and COC angles and the central CO bond length were optimized at the STO-3G level. The outcome illustrated in Figure 2 reveals a significant stabilization of the cis rotamer from 19.9 kcal/mol above trans to 7.9 kcal/mol. Although the central CO bond length only lengthens from 1.437 Å to 1.451 Å upon rotation from trans to cis, the COC and CCO angles are substantially widened from 109.8° and 108.2° to 115.9° and 118.5°, respectively. Single-point 4-31G calculations were then

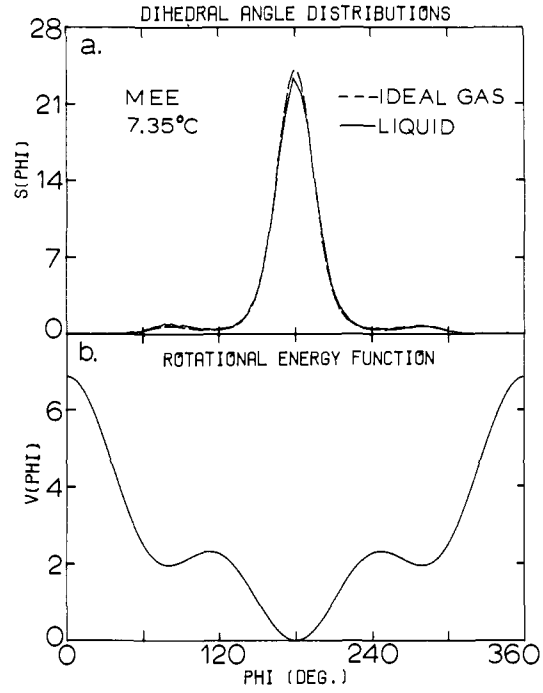

Figure 3. (a) Computed population distributions for the diehedral angle about the central CO bond in MEE. Units for $s(\phi)$ are mole fraction per degree $\times 10^{-3}$. (b) Potential function (eq 2) fit to ab initio results for rotation about the central CO bond in MEE.

performed, using the STO-3G optimized geometries. The results shown in Figure 2 are very similar to the STO-3G data. Finally, the 4-31G energies were fit to the Fourier expansion in eq 2, using

$$V(\phi) = 1/2V_1(1 + \cos\phi) + 1/2V_2(1 - \cos 2\phi) + 1/2V_3(1 + \cos 3\phi) \quad (2)$$

a nonlinear least-squares program. The resultant V_1, V_2, and V_3 and the standard deviation were 4.744, −1.398, 2.139, and 0.10 kcal/mol. The function is illustrated in Figure 3b. Some notable features are the relatively shallow gauche minima in comparison to *n*-butane or DCE[6] and trans to gauche, gauche to trans, and gauche$^+$ to gauche$^-$ barrier heights of 2.33, 0.37, and 4.92 kcal/mol. Furthermore, the trans to gauche energy difference of 1.96 kcal/mol is in reasonable accord with the experimental enthalpy difference of 1.5 kcal/mol obtained from the temperature dependence of IR band intensities in the gas phase.[13a]

Returning to the seemingly anomalous dihedral angle for the gauche conformer, the STO-3G optimizations yielded a value of 85° which the 4-31G results support. With the aid of a referee, it was subsequently discovered that the dihedral angle in MEE has been determined by electron diffraction experiments as (84 ± 6)°.[13b] Prior 4-31G results yielded a value of 70–80°; however the geometries employed were optimized via molecular mechanics and not ab initio calculations.[8b] The trans–gauche energy difference from these computations (2.2 kcal/mol) is in poorer accord with the experimental value than the 4-31G results reported here. This suggests improvement of the geometry for the gauche conformer may be possible in the earlier study.

To explain the anomalous angle, one possibility was that stereoelectronics might be responsible analogous to the popular explanation of the anomeric effect in geminal diethers and carbohydrates.[12,14] Specifically, the constructive two-electron interaction between the π-type lone-pair orbital on oxygen (n_π) and the σ^* orbital of the CC bond would be maximized at a dihedral angle of 90°. Evidence for the anomeric interaction was sought as follows. First, MO drawings for the HOMO's of the trans and

(8) (a) Allinger, N. L.; Chung, D. Y. *J. Am. Chem. Soc.* **1976**, *98*, 6798. (b) Burkert, U. *J. Comp. Chem.* **1980**, *1*, 285.
(9) Radom, L.; Pople, J. A. *J. Am. Chem. Soc.* **1970**, *92*, 4786.
(10) Radom, L.; Lathan, W. A.; Hehre, W. J.; Pople, J. A. *J. Am. Chem. Soc.* **1973**, *95*, 693.
(11) Binkley, J. S.; Whitehead, R. A.; Hariharan, P. C.; Seeger, R.; Pople, J. A.; Hehre, W. J.; Newton, M. D. *QCPE* **1978**, *11*, 368.
(12) (a) Jeffrey, G. A.; Pople, J. A.; Binkley, J. S.; Vishveshewara, S. *J. Am. Chem. Soc.* **1978**, *100*, 373. (b) Jeffrey, G. A.; Taylor, R. *J. Comp. Chem.* **1980**, *1*, 99.
(13) (a) Kitagawa, T.; Miyazawa, T. *Bull. Chem. Soc. Jpn.* **1968**, *41*, 1976. (b) Oyanagi, K.; Kuchitsu, K. *Ibid.* **1978**, *51*, 2237.
(14) (a) Jorgensen, W. L.; Salem, L. "The Organic Chemist's Book of Orbitals"; Academic Press: New York, 1973. (b) David, S.; Eisenstein, O.; Hehre, W. J.; Salem, L.; Hoffmann, R. *J. Am. Chem. Soc.* **1973**, *95*, 3806.

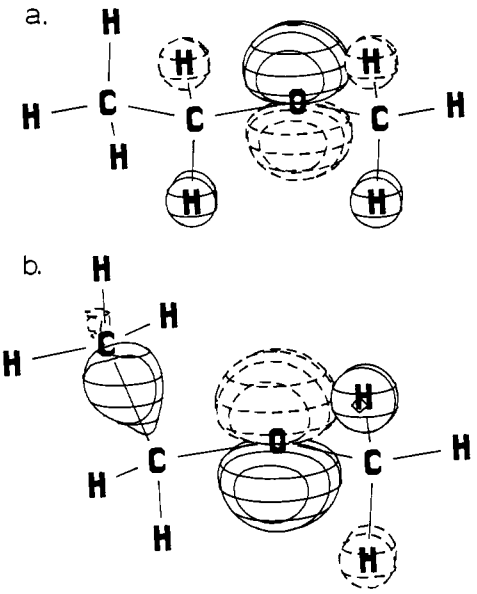

Figure 4. (a) The HOMO for the trans conformer of MEE. See ref 15 for details. (b) The HOMO for the gauche conformer of MEE.

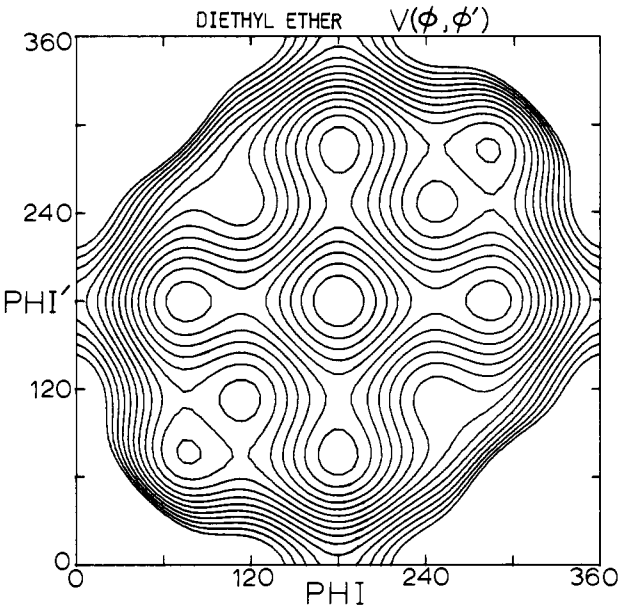

Figure 5. Potential function for internal rotation about the CO bonds in diethyl ether (DEE) fit to ab initio results (eq 3). The innermost contours for the tt, tg, and g^+g^+ minima are 0.5, 2.5, and 4.5 kcal/mol, respectively. The contour increment is 0.5 kcal/mol.

gauche conformers were constructed as shown in Figure 4.[15] The trans HOMO shows out-of-phase mixing with the adjacent π_{CH_2} and π_{CH_3} group orbitals.[14a] The coefficients on the carbons are diminished and those on the hydrogens enhanced by in-phase mixing with the $\pi^*_{CH_2}$ and $\pi^*_{CH_3}$ orbitals. It is not apparent that the gauche HOMO shows greater constructive mixing with antibonding orbitals, though the differences may be below the sensitivity of such drawings. Rather, the out-of-phase mixing between n_π and σ_{CC} is pronounced in the gauche HOMO. The dominance of the latter interaction is consistent with the fact that the STO-3G calculations predict the gauche HOMO to be 0.06 eV higher in energy than the trans HOMO. Second, the anomeric interaction implies enhanced charge transfer from the oxygen to the ethyl group in the gauche conformer. There is slight evidence for this from the population analysis; 0.0015 e is transferred from the oxygen to the ethyl group in going from trans to gauche according to the STO-3G results; however there is charge reorganization of similar magnitude for the 2s and another 2p AO on oxygen as well as the n_π (2p) orbital.

Without the anomeric-like effect, a reasonable explanation is a steric one. In comparing MEE and *n*-butane which has its gauche rotamer at ca. 60°, replacement of the CC bonds in *n*-butane with the shorter CO bonds in MEE creates increased repulsion between the terminal methyl groups in the gauche conformer which is relieved by widening the dihedral angle.

STO-3G calculations were also performed to characterize the rotational potential for diethyl ether. Nine combinations of the two dihedral angles were considered, using the optimized angles from MEE. Optimizations for DEE were not carried out due to the size of the system. 4-31G calculations were also not performed for this reason and since the STO-3G and 4-31G results for MEE were similar. The results were fit to the potential given by eq 3

$$V(\phi,\phi') = V(\phi) + V(\phi') + Ae^{-Br_{15}^2} \qquad (3)$$

where $V(\phi)$ and $V(\phi')$ have the same form as in eq 2. The exponential term is needed to represent the interaction between the terminal methyl groups. The standard deviation for the fit was 0.18 kcal/mol and the constants are V_1 (4.967), V_2 (−1.464), V_3 (2.683), A (236.7), and B (0.4981) when r_{15} is in Å and V in kcal/mol. The function is illustrated by the contour map in Figure 5.

Besides the trans–trans (tt) minimum there are four trans–gauche (tg) and two gauche–gauche (gg) minima. The eclipsed gauche–gauche forms (g^+g^- and g^-g^+) are not minima and are about 8 kcal/mol above tt. The tg minima are 2.1 kcal/mol higher in energy than tt and the g^+g^+ and g^-g^- minima are 4.5 kcal/mol above tt. The only experimental reference is for the tt to tg enthalpy difference which is estimated at 1.4 kcal/mol from IR data in the gas phase.[17]

One computational detail worth noting is that the methyl–methyl distances (r_{15}) used for fitting eq 3 were determined from rigid rotation of the standard TIPS geometry for DEE and differ somewhat from the values in the STO-3G calculations. Thus, although the internal rotations in the liquid simulations are rigid, the rotational potentials are consistent with the monomers being relaxed.

III. Statistical Mechanics of Liquids

A. Ensembles and Averages. Statistical mechanics calculations for liquids are most frequently performed for the canonical ensemble in which the temperature (T), volume (V), and number of particles (N) are fixed. Simulations for a system under the more common experimental condition of constant pressure (P) can also be carried out by using the isothermal–isobaric or NPT ensemble. A concise presentation of the computational formalism for the two approaches has been made by Owicki and Scheraga and will not be repeated here.[18] A key point is that in general the average value of a property Q in the NVT ensemble can be obtained via eq 4 where Q_k is the contribution from the kinetic

$$\langle Q \rangle = Q_k + \int Q(X)P(X)\,dX \qquad (4)$$

$$P(X) = \exp(-\beta E(X)) / \int \exp(-\beta E(X))\,dX$$

$$\beta = (k_B T)^{-1}$$

energy and the configurational integral represents the contributions from the potential energy including intermolecular interactions. $P(X)$ is the Boltzmann factor and the integral is taken over all possible geometric configurations, X, for the system. Equation

$$\langle Q \rangle = Q_k + \int\int Q(X,V)P(X,V)\,dX\,dV \qquad (5)$$

$$P(X,V) = \exp(-\beta H(X,V)) / \int\int \exp(-\beta H(X,V))\,dX\,dV$$

$$H(X,V) = E(X) + PV(X)$$

(15) The drawings were constructed with the PSI/77 program,[16] using STO-3G wave functions and a contour level of 0.09 au.
(16) Jorgensen, W. L. *QCPE* **1978**, *11* 340.
(17) Perchard, J. P.; Monier, J. C.; Dizabo, P. *Spectrochim. Acta, Part A* **1971**, *27A*, 447.
(18) Owicki, J. C.; Scheraga, H. A. *J. Am. Chem. Soc.* **1977**, *99*, 7403.

Table III. Parameters for the Liquid Simulations

ether	ensemble	T, °C	d, g cm^{-3}	no. of configurations, K: equil	no. of configurations, K: averaging	r_{cut}, Å	Δr, Å	$\Delta\alpha$, deg	$\Delta\phi$, deg
dimethyl	NPT	−24.8	(0.724)[a]	200	300	11	0.22	20	
dimethyl	NVT	−24.8	0.737[b]	420	300	10	0.18	18	
methyl ethyl	NVT	7.35	0.720[b]	200	405	11	0.18	18	18
diethyl	NVT	25.0	0.708[b]	470	450	13	0.15	15	15

[a] Calculated. [b] Experimental value, ref 20 and 21.

5 gives the corresponding expressions for the NPT ensemble where V is now a variable. Besides the inter- and intramolecular energy, volume, and enthalpy, numerous distribution functions for the structure and energetics of liquids can be obtained from such averages.

Furthermore, from derivatives of eqs 4 and 5, other thermodynamic properties can be represented as fluctuations in the energy, enthalpy, and volume. The appropriate expressions for the heat capacities, the isothermal compressibility (κ), and the coefficient of thermal expansion (α) are given in eq 6–9.

$$C_V = (\partial\langle E\rangle/\partial T)_V = (\langle E^2\rangle - \langle E\rangle^2)/NkT^2 \quad (6)$$

$$C_p = (\partial\langle H\rangle/\partial T)_p = (\langle H^2\rangle - \langle H\rangle^2)/NkT^2 \quad (7)$$

$$\kappa = -(\partial\langle V\rangle/\partial P)_T/\langle V\rangle = (\langle V^2\rangle - \langle V\rangle^2)/kT\langle V\rangle \quad (8)$$

$$\alpha = (\partial\langle V\rangle/\partial T)_p/\langle V\rangle = (\langle VH\rangle - \langle V\rangle\langle H\rangle)/kT^2\langle V\rangle \quad (9)$$

The critical problem of how to evaluate the configurational integrals was solved by Metropolis et al., using periodic boundary conditions and a sampling algorithm that enables configurations to be picked such that they occur with a probability equal to their Boltzmann factors, $P(X)$ or $P(X,V)$.[18,19] This accelerates convergence of the integrals by avoiding excessive sampling of high-energy configurations whose contribution to the averages is small. With the use of Metropolis sampling the integrals in eq 4 and 5 may be converted to the sum in eq 10 where X' indicates

$$\langle Q\rangle = Q_k + \frac{1}{M}\sum_i^M Q(X'_i) \quad (10)$$

a Metropolis selected configuration. A special feature of the NPT calculations is that N molecule "volume moves" are made in addition to the usual single molecule moves. This is achieved by periodically changing the volume of the periodic cube and scaling the intermolecular separations accordingly.

In running a simulation, several hundred thousand configurations are required typically to equilibrate the system. These are discarded and the final averaging is performed over an additional 10^5–10^7 congiruations depending on the convergence characteristics of the sought properties.

In the simulations with the TIPS, the sampling has included internal rotational degrees of freedom but not vibations in the monomers. Therefore, along with the kinetic energy term the vibrational contributions are considered to be factored out in eq 10. A key item in the simulations is the intermolecular energy of a configuration which is obtained from the pairwise sum of the dimerization energies between all monomers (eq 11). The total

$$E^{inter}(X_i) = \sum_{a<b} \Delta E_{ab} \quad (11)$$

energy is then $E(X_i) = E^{inter} + E^{intra}$ and the enthalpy is $H(X_i) = E(X_i) + PV(X_i)$. Changes in E and H appear in the Boltzmann terms for the Metropolis sampling algorithm in the NVT and NPT ensembles, respectively. Thus, the success of the statistical mechanics calculations depends critically on the quality of the inter- and intramolecular potential functions.

B. Conditions and Variables. The statistical mechanics calculations for the liquid ethers were executed for cubic samples of 128 monomers, using periodic boundary conditions and Metropolis sampling. Simulations in the NVT ensemble were run for DME and MEE at their boiling points (−24.8 and 7.35 °C)[20] and for DEE at 25 °C. The experimental densities were employed as summarized in Table III.[20,21] In addition, an NPT simulation at 1 atm was carried out for DME again at its boiling point to check the computed density. NPT simulations were not run for the other liquids since they are 20–30% slower than the NVT computations. The potential functions described in section II were used throughout. Spherical cutoffs were invoked as usual in evaluating the dimerization energies. As recorded in Table III, the cutoff radii ranged from 10–13 Å which includes interactions with a monomer's 40–50 nearest neighbors. Cutoff corrections to the intermolecular energy were made in the usual manner[3-6] and amounted to less than 0.35 kcal/mol in each case.

New configurations were generated by randomly selecting a monomer, translating it, rotating it about one axis, and performing one internal rotation for MEE and two for DEE. The ranges for the motions were chosen to yield acceptance rates of 40–50% for new configurations and are reported in Table III. For example, the range for the angular moves for DEE was ±15°. The volume changes in the NPT simulation of DME were made on every 250th attempted move. The range for the volume changes was ±300 Å^3 which provided a roughly 50% acceptance rate for the volume moves. Since random numbers are used to determine the exact changes in coordinates for a particular move and the moved molecule, these computations are often referred to as Monte-Carlo simulations. However, the Metropolis procedure is clearly far from random.

The NVT simulations for DME and DEE were initiated from ordered lattices and required 400–500K configurations to equilibrate the inter- and intramolecular energies. The NPT simulation of DME was started from the last configuration in the NVT run and equilibrated within 200 K. Equilibration was also rapid for MEE which was initiated from a modified configuration of *n*-butane[6] which has a comparable molecular volume. Final averaging took place over an additional 300–450K configurations as summarized in Table III.

IV. Results and Discussion

A. Dimethyl Ether. The results of the liquid simulations for DME will be presented first since it is the protypical system and reveals the principal structural features for the liquid ethers. Emphasis is placed on comparison of the NVT and NPT results. In fact, the NPT simulation of liquid water by Owicki and Scheraga appears to be the only other NPT study of a molecular liquid besides diatomics.[18] Thus, such comparisons have not been made previously.

i. **Thermodynamics.** The thermodynamic results from the two simulations are compared with the available experimental data in Table IV. The standard deviations (2σ) reported here for computed quantities are obtained from separate averages over each increment of 15–25K configurations.

Overall, the computed results are very similar being within 5–10% of each other. Most significantly the computed density from the NPT simulation is only 3% below the experimental value.

(19) Metropolis, N.; Rosenbluth, A. W.; Rosenbluth, M. N.; Teller, A. H.; Teller, E. *J. Chem. Phys.* **1953**, *21*, 1087.

(20) "Selected Values of Properties of Chemical Compounds", Thermodynamics Research Center Data Project, Texas A&M University: College Station, TX, 1980.

(21) (a) Maass, O.; Boomer, E. H. *J. Am. Chem. Soc.* **1922**, *44*, 1709. (b) Aronovich, K. A.; Kastorskii, L. P.; Fedorova, K. F. *Zh. Fiz. Khim.* **1967**, *41*, 20.

(22) Kennedy, R. M.; Sagenkahn, M.; Aston, J. G. *J. Am. Chem. Soc.* **1941**, *63*, 2267.

Table IV. Thermodynamic Results for Liquid Dimethyl Ether at −24.8 °C

property	calculated NPT	calculated NVT	exptl
V, Å^3/molecule	107.3 ± 0.6	(103.8)[a]	103.8,[b] 104.2[c]
d, g cm^{-3}	0.713 ± 0.004	(0.737)[a]	0.737,[b] 0.735[c]
E^{inter}, kcal/mol	−4.96 ± 0.03	−5.10 ± 0.02	
ΔH_V^0, kcal/mol	5.45	5.59	
ΔH_V, kcal/mol	5.40	5.54	5.14[d]
C_p^{inter}, cal/(mol deg)	6.3 ± 1.5		
C_p, cal/(mol deg)	20.2		24.7[d]
C_V^{inter}, cal/(mol deg)		4.0 ± 0.9	
C_V, cal/(mol deg)		16.0	
κ, atm^{-1} × 10^{-6}	92 ± 25		
α, deg^{-1} × 10^{-5}	87 ± 25		(187)[b,c]

[a] Assumed. [b] Reference 21a. [c] See text. [d] Reference 22.

In conjunction with the computed heat of vaporization which is within 5% of the experimental value, the results support the validity of the TIPS representation of the intermolecular interactions.

Some details of the results require comment. (1) The experimental density of 0.737 g cm^{-3} is based on the data nearest the boiling point;[21] however plotting the density data for the entire range vs. temperature shows the point nearest the boiling point is uniquely off-line. On the basis of the straight line, the density should be 0.735 g cm^{-3} which yields a molecular volume of 104.2 Å^3. (2) ΔH_V^0 is the enthalpy of vaporization for the liquid going to the ideal gas. It is computed from $\Delta H_V^0 = \Delta E_V^0 + P(V(\text{ideal gas}) - V(\text{l}))$ where $\Delta E_V^0 = E(\text{ideal gas}) - E(\text{l}) \approx -E^{inter}(\text{l})$ for DME.[3-6] (3) ΔH_V and ΔH_V^0 are related by the enthalpy departure function for the real gas: $\Delta H_V = \Delta H_V^0 - (H^0 - H)$. $H^0 - H$ is calculated from virial coefficient data and the expression from the virial equation of state.[6] Since DME yields a relatively ideal gas the correction is only 0.05 kcal/mol at −24.8 °C. (4) The heat capacities of such liquids are dominated by the contributions from the kinetic and vibrational energy of the monomers. This is best approximated by the heat capacity of the ideal gas, C_P^0 or C_V^0, which is available in compilations.[23] The heat capacities of the liquid may then be estimated by adding the computed intermolecular contribution, C_P^{inter} or C_V^{inter}, to the ideal gas values. The resultant C_P for DME, 20.2 cal/(mol deg), is in reasonable agreement with the experimental values, 24.7.[22] (5) The compressibility and expansivity were also computed in the NPT simulation according to eq 8 and 9. The nature of the expressions leads to substantial error bars for the computed results. Further study is required to ascertain the length of runs needed to assure convergence of these quantities. It is well known that fluctuation properties including the heat capacities converge much more slowly than energies or radial distribution functions.[24] Nevertheless, the computed κ and α at least have the right order of magnitude for organic liquids. An experimental α of 187 × 10^{-5} deg^{-1} for DME was estimated from the linear relationship for density vs. temperature mentioned above. Some of the discrepancy with the computed α may be due to the fact that a correction for a unimolecular contribution to α needs to be made for the neglected vibrations as for C_P. An experimental value for the compressibility of DME could not be found.

ii. **Structure.** Radial distribution functions (RDF's) represent the deviations in the distributions of atoms in a liquid from the bulk density values. The density of y atoms at a distance r from an atom of type x is $\rho_{xy}(r) = \rho^0_y g_{xy}(r)$ where ρ^0_y is the bulk density (N_y/V) and $g_{xy}(r)$ is the xy RDF. Consequently, peaks in the RDF's are often assigned to intermolecular structural features such as solvation shells. Although the RDF's can be determined from diffraction experiments, extraction of the individual atomic RDF's from the total distribution functions is difficult. No diffraction results appear to be available for liquid ethers.

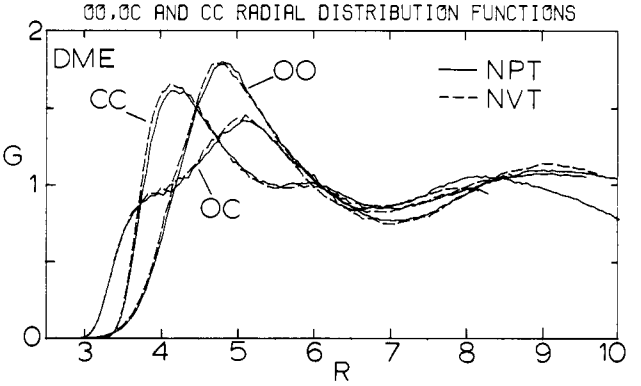

Figure 6. Computed intermolecular OO radial distribution functions (RDF's) from the NPT and NVT simulations of liquid DME. Distances are in Å throughout.

Table V. Thermodynamic Results for Liquid Methyl Ethyl Ether at 7.35 °C and Diethyl Ether at 25 °C[a]

property	MEE	DEE
E^{inter}	−5.88 ± 0.03	−6.76 ± 0.05
E^{rot}	0.47 ± 0.01 (0.45)[b]	0.97 ± 0.03 (0.93)[b]
ΔH_V^0	6.42	7.31
ΔH_V	6.36 (5.91)[c]	7.22 (6.51)[c]
C_V^{inter}	4.2 ± 0.8	5.3 ± 1.4
C_V	24.8	31.3 (41.4)[c,d]
% trans gas	93.9[b]	94.8[b]
% trans liquid	92.9 ± 0.6	93.4 ± 0.4

[a] Units are the same as in Table IV. [b] Ideal gas values obtained from Boltzmann distributions for eq 2 and 3. [c] Experimental value, ref 20. [d] Experimental C_p.

The computed OO, OC, and CC RDF's from the NVT and NPT simulations are compared in Figure 6. Consistent with the thermodynamic results, the RDF's are nearly identical in each case. A small shift of some of the peak positions to larger r in the NPT case is apparent. This is in line with the slightly lower density. The earlier tail off of the CC RDF for the NVT results is not significant, but is due to the 1 Å shorter cutoff employed in that run. The cutoff is based on the OO separations.

The broad, low peaks in the RDF's are typical of non-hydrogen-bonded organic liquids.[6] The position of the first peak in g_{OO} is consistent with the potential curves in Figure 1. Clearly, no monomers can approach within an OO distance of about 3.5 Å. Integration of the peak out to 7 Å yields 13 neighbors in this range. The most intriguing feature in the RDF's is the shoulder in g_{OC} at about 3.8 Å. Integration indicates that each monomer has an average of about 4 OC and CO interactions within 4 Å. Thus, on this basis 4 of a monomer's ca. 13 neighbors seem a little special. Though it is tempting to conjure up remnants of a water-like structure, this is not supported by analysis of stereoplots of configurations from the simulations of DME. An example is provided in Figure 7. In viewing such drawings the periodicity of the system should be kept in mind; monomers near one face are also proximate to those on the opposite face. Although most monomers appear to be engaged in several constructive OC and CO interactions, many Coulombically less favorable CC interactions are evident at comparable distances. This is supported by the location of the first peak for g_{CC} shown in Figure 6. Nevertheless, some influence of the Coulombic interactions is evident for liquid DME in the shorter OC than OO contacts (Figure 6). However, the structuring is feeble in comparison to water where the much

(23) Reid, R. C.; Prausnitz, J. M.; Sherwood, T. K. "The Properties of Gases and Liquids"; McGraw-Hill: New York, 1977; 3rd ed.

(24) (a) Mezei, M.; Swaminathan, S.; Beveridge, D. L. *J. Chem. Phys.* **1979**, *71*, 3366. (b) Pangali, C.; Rao, M.; Berne, B. J. *Chem. Phys. Lett.* **1978**, *55*, 413.

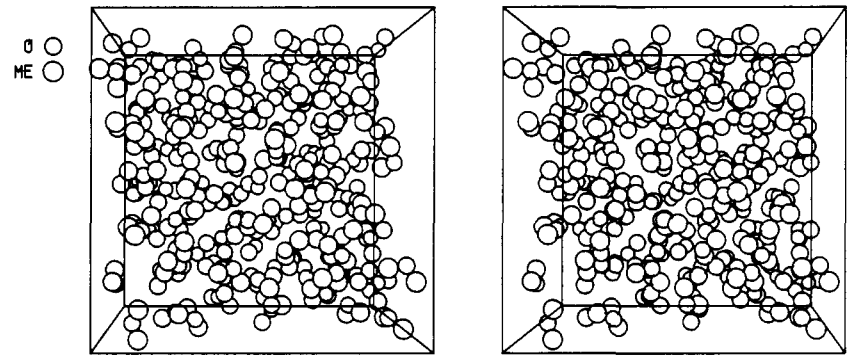

Figure 7. Stereoplot of a configuration from the NPT simulation of liquid DME. The periodic cube contains 128 monomers.

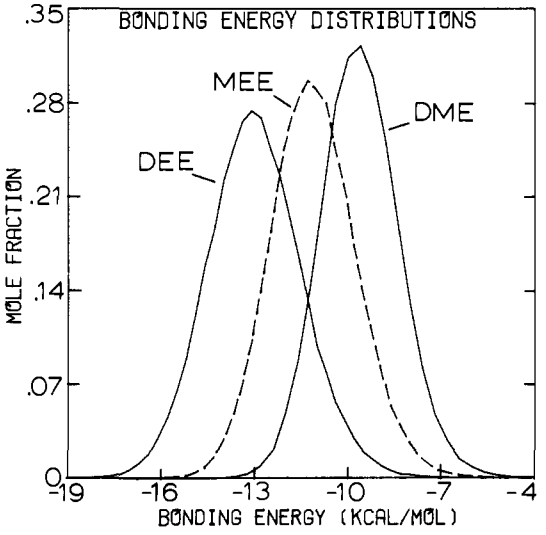

Figure 8. Computed distributions of intermolecular bonding energies for monomers in the three liquids. The units for the ordinate are mole fraction per kcal/mol.

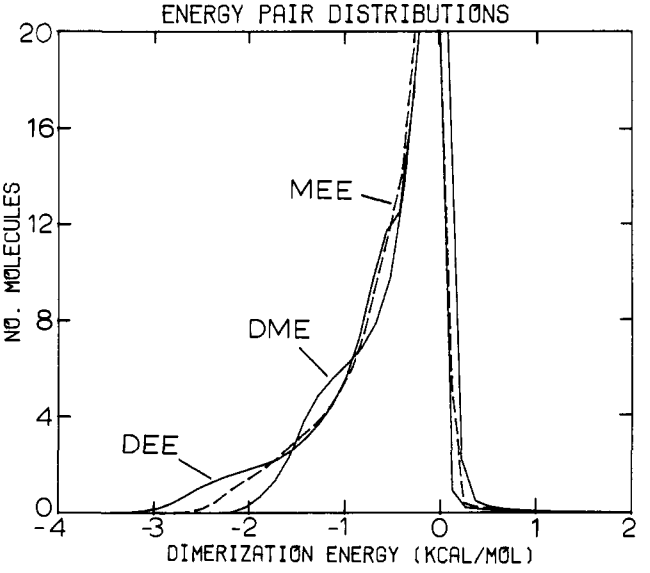

Figure 9. Computed distributions of dimerization energies for a monomer in each of the three liquids. The units for the ordinate are molecules per kcal/mol.

stronger Coulombic forces yield the stricking hydrogen-bonded network.[3,25]

B. **Methyl Ethyl Ether and Diethyl Ether.** i. **Thermodynamics and Energy Distributions.** The thermodynamic results from the NVT simulations for liquid MEE and DEE are given in Table V. The computed heats of vaporization are again in good agreement with experiment. For all three ethers ΔH_V is overestimated by 7–11%. It should be noted that in computing ΔH_V for a system including internal rotation, $\Delta E_V^0 \approx E^{rot.}$ (ideal gas) $- (E^{inter}(l) + E^{rot.}(l))$ where $E^{rot.}$ is the intramolecular rotational energy.[6] The ideal gas values for $E^{rot.}$ were obtained from Boltzmann distributions for eq 2 and 3.

The computed C_V's also seem reasonable, though there are no experimental data for comparison. Again, they are dominated by the unimolecular contributions.

The energetic environments of the monomers in the liquids were also monitored during the simulations. The distributions of total intermolecular bonding energies for monomers in the NVT calculations are contrasted in Figure 8. In each case the monomers experience an energetic continuum of environments with substantial ranges. The intermolecular bonding is progressively strengthened as the monomers are elaborated due to the greater van der Waals attraction between the larger monomers. Of course, this is manifested in the increasingly higher ΔH_V's as the monomers grow. The greater range of interactions for larger monomers in Figure 8 is partly due to the 50 °C increase in temperature for the simulations in going from DME to DEE.

The energy pair distributions from the NVT calculations are shown in Figure 9. The ordinate records the average number of molecules that are bound to a monomer with the dimerization energy given on the abscissa. The spikes near 0 kcal/mol are due to the many molecules in the bulk far from the reference monomer, while the shoulders at low energy represent particularly constructive interactions with near neighbors. Again, due to the greater dispersion attraction the larger monomers show stronger bonding to near neighbors. Naturally, the minima in the TIPS determine the lowest possible dimerization energies. Thus, Figure 9 indicates the most favorable intermolecular interaction in liquid DME is around 2 kcal/mol which is consistent with Figure 1 and Table II.

The dimerization energies for the liquid ethers are smoothly distributed with no sharp dividing line between the near neighbors and the bulk. However, the distributions do seem to change slope around −1 kcal/mol. Integration to this point yields 4–5 neighbors in each case. This is the same as the number of short OC and CO interactions in DME(l). So, it appears that each monomer does have a few interactions with neighbors that particularly benefit from the Coulombic attractions. For hydrogen-bonded liquids the distinction between the hydrogen-bonded neighbors and the bulk is pronounced yielding bimodal energy pair distributions.[3-5,25]

ii. **Internal Rotation.** The computed distribution functions for the dihedral angle, $s(\phi)$, in MEE are shown in Figure 3a. The distributions for the ideal gas and the liquid are nearly identical so there is no significant condensed phase effect on the trans–gauche conformational equilibrium at the normal liquid density. This is in agreement with IR data which yield the same trans–gauche enthalpy difference for both the gas and pure liquid MEE.[13] The trans populations are obtained by integrating $s(\phi)$ from 120° to 240°, the remainder being gauche. As recorded in Table V, the results are 93.9% trans for the ideal gas and 92.9 ± 0.6% for liquid MEE at 7.35 °C. The trans populations in liquid

(25) Jorgensen, W. L. *Chem. Phys. Lett.* **1980**, *70*, 326.

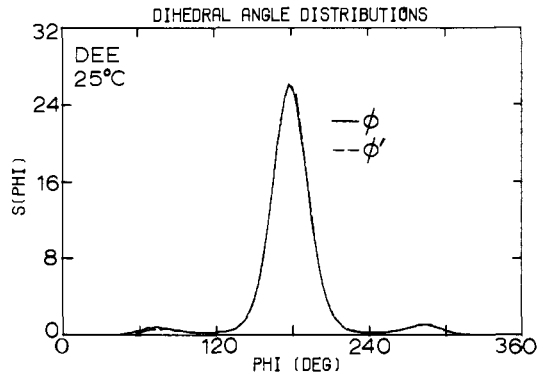

Figure 10. Individual dihedral angle distributions computed for the two dihedral angles of DEE monomers in the liquid.

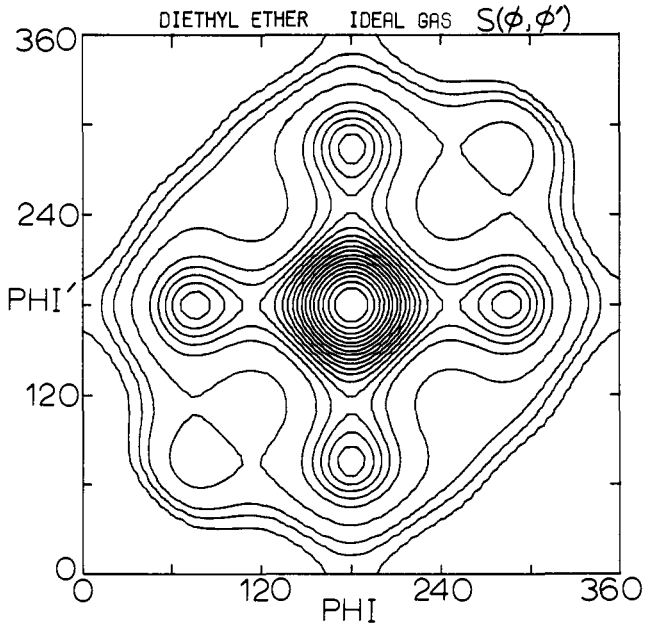

Figure 11. Contour map for the distribution function, $s(\phi,\phi')$, for the dihedral angles of DEE in the ideal gas phase computed from a Boltzmann distribution for eq 3. The 20 contour levels increase steadily along the diagonal from ϕ,ϕ' of 360°,360° to 180°,180°. There are four tg and one tt maxima.

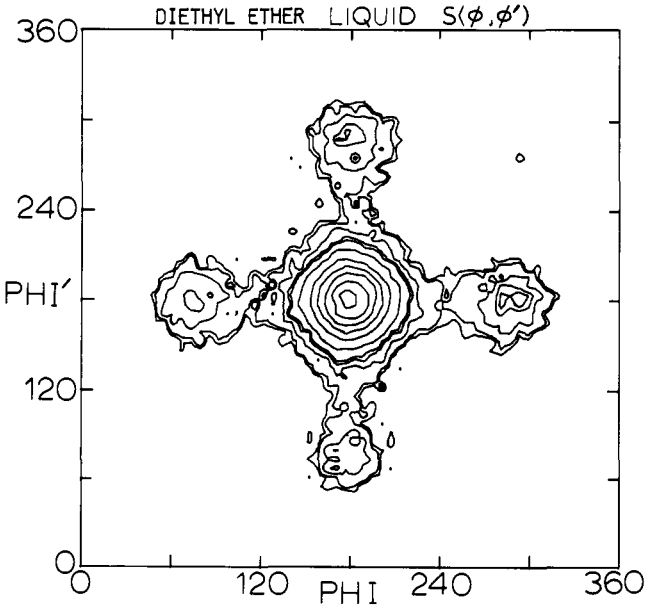

Figure 12. Contour map for $s(\phi,\phi')$ as in Figure 13 computed for liquid DEE.

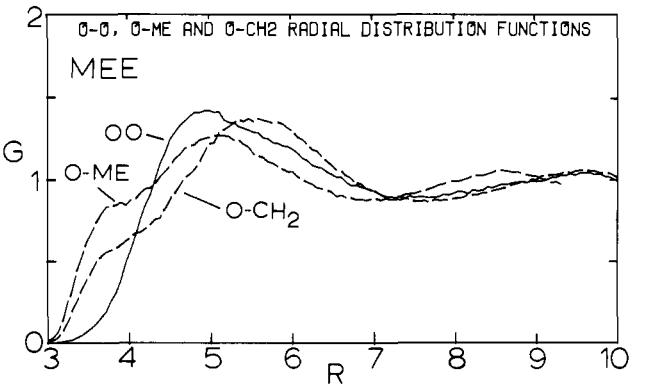

Figure 13. Computed intermolecular RDF's for liquid MEE. The O–ME distribution refers to the methoxy methyl group.

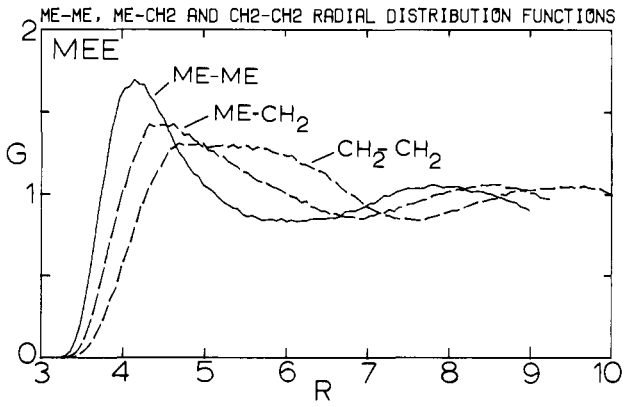

Figure 14. Computed intermolecular RDF's for liquid MEE involving the methoxy methyl group (ME).

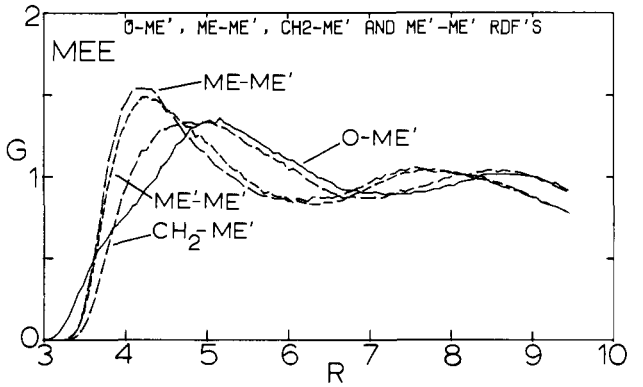

Figure 15. Computed intermolecular RDF's for liquid MEE involving the ethoxy methyl group (ME').

n-butane at −0.5 °C (67%) and in DCE at 25 °C (44%) are substantially less owing to the deeper and lower gauche potential wells in these cases.[6] Furthermore, DCE is remarkable since it is the only pure liquid that has been modeled so far which shows a pronounced condensed phase effect on $s(\phi)$. The charge distribution and concomitant Coulombic interactions for DCE were shown to be responsible for the enhanced gauche population in the liquid.[6] The dialkyl ethers have charge distributions similar to simple alcohols with the negative oxygen between two positive atoms. Since the groups β to the oxygen are roughly neutral their orientation does not affect the electrostatic interactions between neighbors. Consequently, neither the simple ethers nor alcohols[4,5] show condensed phase effects on $s(\phi)$. However, shifts in the conformational equilibria for polyoxygenated compounds can be anticipated. For example, the oxygens and methylenes in 1,2-dimethoxyethane have the same charge pattern as a DCE monomer in the TIPS model. Thus, an increase in the gauche population for the central CC bond in 1,2-dimethoxyethane is predicted in going from the gas phase to the pure liquid.

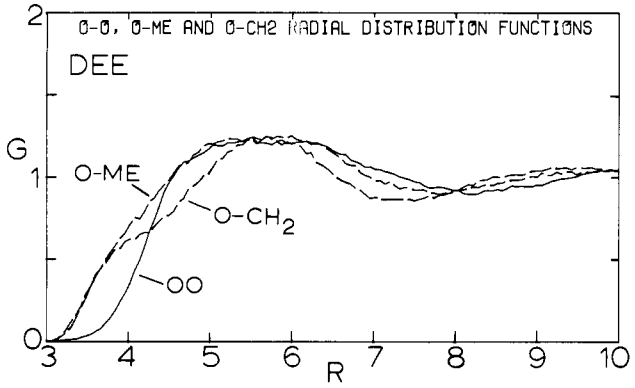

Figure 16. Computed intermolecular RDF's for liquid DEE involving oxygen.

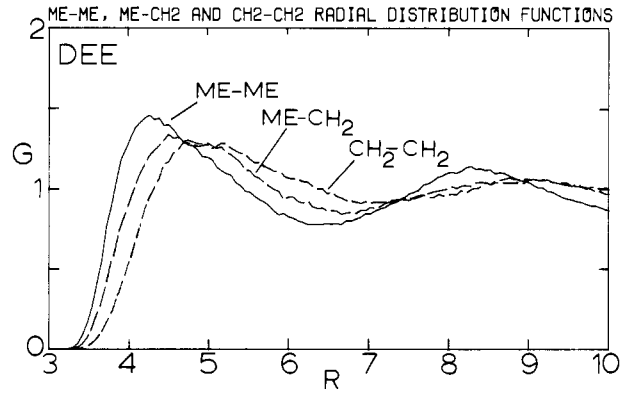

Figure 17. Computed intermolecular RDF's between alkyl groups for liquid DEE.

The separate distributions for the two CCOC dihedral angles in liquid DEE are presented in Figure 10. The overall trans populations given in Table V are similar to the results for MEE and again show no significant condensed phase effect. The identicality of the distributions for ϕ and ϕ' in Figure 10, the symmetry of the distributions in Figures 3a and 10, and the small standard deviations for the trans populations and rotational energies fully support the convergence of the conformational results. Moreover, the starting configurations for the simulations had highly non-Boltzmann distributions for $s(\phi)$ and $s(\phi,\phi')$. Specifically, the initial gauche population for MEE was ca. 32% and the simulation of DEE started with the monomers all in the cis,cis conformation. Equal numbers of trans to gauche and gauche to trans barrier crossings were also obtained during the averaging which confirms the conformational equilibration. Gauche to gauche transitions did not occur.

The two-dimensional distribution, $s(\phi,\phi')$, for DEE in the ideal gas state is shown in Figure 11 as obtained from a Boltzmann distribution for eq 3. The figure clearly reflects the tt and tg minima from Figure 5. Due to memory space considerations, $s(\phi,\phi')$ for the liquid was not obtained directly during the averaging. However, it could be partly constructed from configurations that were saved every ca. 2000 attempted moves during the Monte-Carlo run. The result is shown in Figure 12 where the resolution is poor due to the truncated data base of only about 200 configurations. Integration of the distributions yields tt and tg populations of 89.7% and 10.3% for the ideal gas and 86.9% and 13.1% for liquid DEE at 25 °C. Since these numbers sum to 100%, no other conformers are present appreciably which is in accord with IR data.[17]

iii. **Structure.** The computed RDF's for liquid MEE and DEE are displayed in Figures 13–17. There are ten unique RDF's for MEE and only six for DEE in view of the higher symmetry. In Figures 13–15, ME refers to the methoxy methyl group and ME′ is the ethoxy methyl group for MEE. There are many similarities with the RDF's for DME. First, the shoulder near 3.8 Å in g_{OC} for DME is again found in the O–ME and O–CH_2 RDF's for MEE and the O–CH_2 RDF for DEE. These Coulombically favorable interactions yield the shortest intermolecular separations along with the methyl–methyl contacts. Close approach of oxygens is avoided; the g_{OO}'s all have their first maximum near 5 Å.

Overall, there are indications of a general reduction in structure in progressing from DME to DEE. This is reflected in the broadening and lowering of the peaks for the liquids with the larger monomers as in the O–O, O–ME, and O–CH_2 RDF's in Figures 6, 13, and 16. Such a trend seems reasonable since dispersion is increasingly dominant for the larger monomers and diminishes the importance of the Coulomb terms in structuring the liquids. However, the temperature change in the simulations is also

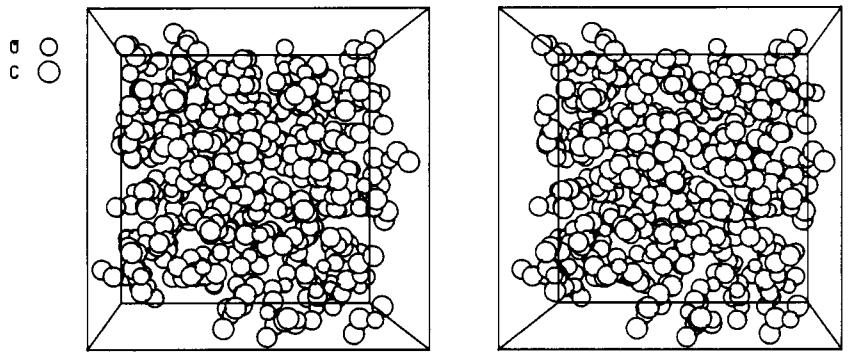

Figure 18. Stereoplot of a configuration from the simulation of liquid MEE. The cube contains 128 monomers.

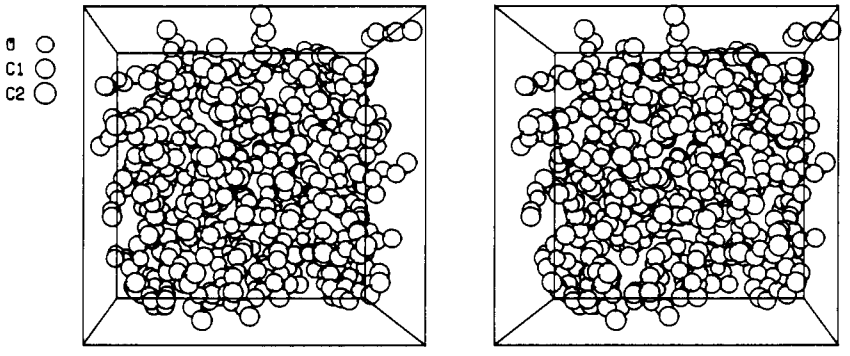

Figure 19. Stereoplot of a configuration from the simulation of liquid DEE. The cube contains 128 monomers.

contributing to the reduction in structure for MEE and DEE.

Stereoplots of configurations from the simulations of liquid MEE and DEE are shown in Figures 18 and 19. The liquids are disordered with no obvious repeating polymeric units or especially favored dimer geometries. The axes of the monomer chains point in all directions so no alignment of the chains is evident. And, in keeping with dihedral angle distributions gauche bonds are rare. Coordination numbers are high in both cases and hard to estimate unequivocally. However, integrating the first peaks in g_{OO} to their minima at 7.4 Å for MEE and 8.3 Å for DEE yields 12 and 13 neighbors, respectively. Thus, the number of neighbors appears to remain constant for the series which is reasonable since the size of the reference monomer (the solute) and its neighbors (the solvent molecules) are growing at the same rate.

V. Conclusion

This work represents the most extensive theoretical treatment to date of liquid alkyl ethers. It also illustrates the quality of results and detailed insights into the structures and properties of complex organic liquids that can be obtained from statistical mechanics simulations. In this and earlier papers[4-6] it has been demonstrated that our theoretical approach is a particularly valuable means for studying internal rotation in pure liquids. The agreement between the computed and experimental thermodynamic properties for the liquid ethers including the density of DME also supports the viability of the TIPS model for representing intermolecular interactions. The additional data available from simulations in the NPT ensemble and the closer tie to the usual experimental conditions make this the procedure of choice for future work. It will be particularly interesting to study the pressure dependence of the structures, properties, and conformational equilibria for pure liquids and dilute solutions.

Acknowledgment. Gratitude is expressed to the National Science Foundation (CHE7819446) for financial assistance. Acknowledgment is also made to the donors of the Petroleum Research Fund, administered by the American Chemical Society, for support of this work. Dr. Phillip Cheeseman kindly provided the program to make the stereoplots. The authors are also grateful to Yarmouk University, Irbid, Jordan, for a fellowship granted to M.I. and to Professor B. J. Zwolinski for providing thermochemical data.[20]

Geometry and Electronic Structure of $(CO)_3NiCH_2$. A Model Transition-Metal Carbene

Dale Spangler,[†] John J. Wendoloski,[†] Michel Dupuis,[†] Maynard M. L. Chen,[‡] and Henry F. Schaefer III*[‡]

Contribution from the National Resource for Computation in Chemistry, Lawrence Berkeley Laboratory, University of California, Berkeley, California 94720, and Department of Chemistry and Lawrence Berkeley Laboratory, University of California, Berkeley, California 94720.
Received May 19, 1980

Abstract: The first application of nonempirical molecular electronic structure theory to a realistic transition-metal carbene complex is reported. The system chosen was $(CO)_3NiCH_2$, methylene(tricarbonyl)nickel(0). All studies were carried out at the self-consistent-field (SCF) level. A large and flexibly contracted basis set was chosen, labeled Ni(15s 11p 6d/11s 8p 3d), C,O(9s 5p/4s 2p), H(5s/3s). The critical predicted equilibrium geometrical parameters were R[Ni–C(methylene)] = 1.83 Å, θ(HCH) = 108°. The sixfold barrier to rotation about the Ni–C(methylene) axis is small, ~0.2 kcal. The electronic structure of $(CO)_3NiCH_2$ is discussed and compared with those of the "naked" complex $NiCH_2$ and the stable $Ni(CO)_4$ molecule.

A critical ingredient in the flowering of organometallic chemistry over the past decade has been the synthesis and characterization of transition-metal carbene complexes.[1-6] This research began with the report in 1964 by Fischer and Maasböl[8] of methoxymethylcarbene(pentacarbonyl)tungsten. Although the notion of a double bond between transition metals and carbon was initially unorthodox, it is now very well entrenched and indeed an integral part of the thought patterns of organometallic researchers. In fact, metal carbene concepts borrowed from organometallic chemists are now being used in attempts to understand surface chemistry and heterogeneous catalysis.[8-12]

A primary motivation for the construction of such an analogy has been the growing consensus[13-15] that transition-metal carbenes are homogeneous catalysts in the olefin metathesis reaction.

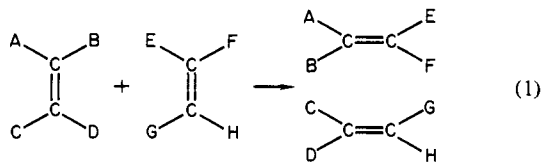

(1)

Of the two mechanisms often considered for the olefin metathesis reactions, one involves the pairwise exchange between two olefins in the coordination sphere of a metal, while the other is the "carbene chain reaction" in which a carbene–metal complex is the active catalyst. Experimentally, isomerization patterns and

[†] National Resource for Computation in Chemistry.
[‡] Department of Chemistry.

(1) Fischer, E. O. *Adv. Organomet. Chem.* **1976**, *14*, 1.
(2) Schrock, R. R.; Parshall, G. W. *Chem. Rev.* **1976**, *76*, 243.
(3) Fischer, E. O.; Schubert, V.; Fischer, H. *Pure Appl. Chem.* **1977**, *50*, 857.
(4) Casey, C. P.; Burkhardt, T. J.; Bunnell, C. A.; Calabrese, J. A. *J. Am. Chem. Soc.* **1977**, *99*, 2127.
(5) Herrmann, W. A. *Angew. Chem., Int. Ed. Engl.* **1978**, *17*, 800.
(6) Wood, C. D.; McLain, S. J.; Schrock, R. R. *J. Am. Chem. Soc.* **1979**, *101*, 3210.
(7) Fischer, E. O.; Maasböl, A. *Angew. Chem., Int. Ed. Engl.* **1964**, *3*, 580.
(8) Mason, R. *Israel J. Chem.* **1977**, *15*, 174.
(9) Schaefer, H. F., III *Acc. Chem. Res.* **1977**, *10*, 287.
(10) Muetterties, E. L. *Angew. Chem., Int. Ed. Engl.* **1978**, *17*, 545.
(11) Yates, J. T.; Worley, S. D.; Duncan, T. M.; Vaughan, R. W. *J. Chem. Phys.* **1979**, *70*, 1225.
(12) Gavezzotti, A.; Simonetta, M. *Chem. Phys. Lett.* **1979**, *61*, 435.
(13) Katz, T. J. *Adv. Organomet. Chem.* **1977**, *16*, 283.
(14) Calderon, N.; Lawrence, J. P.; Ofstead, E. A. *Adv. Organomet. Chem.* **1979**, *17*, 449.
(15) Grubbs, R. H. *Prog. Inorg. Chem.* **1978**, *24*, 1.

0002-7863/81/1503-3985$01.25/0